Chemistry Research Journal, 2023, 8(4):20-36
Available online www.chemrj.org

Research Article

ISSN: 2455-8990
CODEN(USA): CRJHA5

Synthesis of Zinc Nanoparticles using Stem Extract of *Punica granatum* and its Applications

Prema Alagar[1], Muthuselvi R[2*], Vasantha R[3]

[1]Research Scholar, School of Chemistry, Madurai Kamaraj University, Madurai (TN), India-625 021
[2]Assistant Professor, Sri Meenakshi Government Arts College for Women (A), Madurai (TN), India-625 002
[3]Assistant Professor, Anna Adarsh College for Women, Chennai (TN), India – 600 040
*Corresponding author. E-mail: : muthuselviumashankar@gmail.com

Abstract
Plant components such as flavonoids, terpenoids, polyphenols, alkaloids, and others are used as reducing agents during the biogenic synthesis of zinc nanoparticles (ZnNPs). Due to its anticancer and antimicrobial property, plant-mediated green production of zinc nanoparticles (ZnNPs) attracted more attention. The aqueous stem extract of Punica granatum (PG) and its useful properties were used in the current study to develop a new, more environmentally friendly method of producing zinc nanoparticles (ZnNPs). The zinc acetate solution is reduced to zinc in the current work by an aqueous stem extract of Punica granatum (PG), which also serves as a capping agent. Colour changes proved the nanoparticles were synthetic. UV-Vis spectroscopy, FTIR, SEM-EDAX, TEM, XRD, TGA, DTA, and BET were used to analyse newly synthesised nanoparticles. According to measurements made by TEM and SEM, nanoparticle sizes generally fell between 11 and 30 nm. Additionally, ZnNPs effectiveness in preventing the growth of various pathogenic microorganisms was assessed using the disc diffusion method, and their effectiveness as anticancer agent was investigated with HeLa and SKMEL-3 cells.

Keywords: Punica granatum (PG) stem, ZnNPs, SEM-EDAX, XPS, microbial, anticancer

1. Introduction

A fascinating field in nanoscience and technology over the past ten years has been the development of new synthesis techniques for nanomaterials, such as metal nanoparticles, quantum dots (QDs), carbon nanotubes (CNTs), graphene, and their composites [1–9]. Today, nanotechnology is regarded as a validated state-of-the-art technology with a wide range of applications in the chemical, pharmaceutical, mechanical, and food processing industries. Large surface area to volume ratio nanoparticles are becoming more and more important in industry due to their small size. The study of inorganic nanoparticles, such as metallic nanoparticles, oxide nanoparticles, sulphide nanoparticles, and other common nanoparticles, through biosynthesis has grown significantly. There are numerous physical, chemical, biological, and hybrid techniques that can be used to create nanoparticles. In order to create nanoparticles, physical and chemical procedures are more common, but their usage has been constrained by their toxicity. Due to the ease of use and adaptability of the processes, there is presently increased interest in the development of safe, environmentally friendly techniques of biogenetic production. The preferred tool is green nanoparticle synthesis, which is simple to manufacture and create. Recent years have seen a lot of attention from scientists on the development of environmentally friendly processes for synthesising nanoscale materials. An

alternative to chemical synthesis is emerging: plant-based green synthesis. The most abundant source of bio-active organic compounds, such as polyphenols, flavonoids, alkaloids, terpenes, and tannins, are found in plants. An emerging trend is the green synthesis of nanoparticles, which is thought to be easy, inexpensive, and non-toxic, especially when plant extracts from various species are used. Compared to other nanoparticles, metal nanoparticles are used more frequently for therapeutic purposes (Sanita Banerjee, 2012). Zinc nanoparticles stand out among metal nanoparticles due to their distinctive optical and chemical behaviours that can be easily controlled by altering the shape. Modern uses for zinc nanoparticles can be found in the fields of electronics, communication, sensors, cosmetics, biology, and the pharmaceutical industry [10–14].

Furthermore, biological applications like biological sensing, drug delivery, and nanomedicines hold great promise for zinc nanoparticles. Ahmad et al. used Pomegranate peel extract and the biowaste of the fruit to biosynthesize silver and gold nanoparticles at room temperature. Transmission electron microscopy (TEM), selected area electron diffraction (SAED), and X-ray diffraction (XRD) spectra were used to assess the NPs' shape. Silver and gold nanoparticles had typical particle sizes of 5 1.5 nm and 10 1.5 nm, respectively. Aqueous pomegranate leaf extract was used by Nisha et al. to create nanoparticles, which were then verified by FTIR, XRD, FTIR-SEM with EDAX, and UV-visible spectra at 437nm. Pathogens such as Pseudomonas, Bacillus cereus, Staphylococcus albus, and Proteus were tested for antibacterial activity. Utilising pomegranate leaf, flower, and fruit extracts, Vennila et al. observed the decrease of pure Ag++ ion. Sharp bands were visible in the UV spectrum between 350 and 400nm for leaves and 450 and 490nm for flowers and fruits. By using the conventional disc diffusion method, antibacterial experiments against Gram positive (Staphylococcus aureus) and Gram negative (Pseudomonas) strains as well as two harmful fungus, Candida albicans and Aspergillus, were also carried out. Using Punica granatum peel extract, Kaur et al. produced copper nanoparticles (CuNPs) physiologically. FTIR and TEM were used to characterise the synthesised nanoparticles. This revealed that the particles were between 15 and 20nm in size. It was discovered which bacteria had in vitro antibacterial activity against Micrococcus luteus MTCC 1809, Pseudomonas aeruginosa MTCC 424, Salmonella enterica MTCC 1253, and Enterobactor aerogenes MTCC 2823. The typical particle size ranges between 5 and 50 nm, according to Shanmugavadivu et al.'s silver nanoparticles, which were produced using pomegranate peel extract and characterised by UV-Vis spectrum [371nm], FTIR, and SEM analysis. AgNPs antibacterial effects on the pathogens Staphylococcus aureus, Pseudomonas aeruginosa, and Escherichia coli were assessed. Shalinie et al. showed green synthesis of silver nanoparticles from the extract of pomegranate fruit seeds in their study phytofabrication of silver nanoparticles utilising pomegranate fruit seeds. Using the TEM and XRD methods, the morphology of the synthesised nanoparticles was identified. When tested against various human diseases with multidrug resistance, the synthesised nanoparticles were found to be extremely hazardous. The manufacture of zinc nanoparticles (ZnNPs) using biosynthetic and environmentally friendly technology is thought to be nontoxic, bio safe, and biocompatible, and the nanoparticles have been used as medication carriers, cosmetics, and fillers in medical materials (Rosiand Mirkin, 2005).

However, compared to silver nanoparticles, the majority of Zn-nanoparticles utilised in commerce have some advantages, such as being less expensive and appearing whiter (Vigneshwaran, 2006). As a quick and practical substitute for chemical and physical procedures, the utilisation of plant extracts in the biosynthetic process has attracted interest (Singh, 2011).

In the current study, we have concentrated our attention on the stem of the Punica Granatum plant, which is frequently consumed by humans as food and has a variety of traditional purposes for the treatment of ailments. Therefore, utilising the aqueous stem extracts of Punica granatum, we present a straightforward and unique plant-based production of zinc nanoparticles. Zinc nanoparticles (ZnNPs) produced through green synthesis have a number of biomedical applications. The Punica granatum aqueous stem extract contains metabolites that function as a capping and reducing agent for the biogenic synthesis of ZnNPs. Modern methods like UV spectroscopy, FTIR, SEM-EDAX, TEM, XRD, TGA, DTA, BET, and XPS were used to analyse the green synthesised nanoparticles. Novel ZnNPs that has been synthesised has good anticancer activity and antimicrobial efficacy. The possibility for using plant-based NPs in the biomedical industry will grow as a result of this research.

2. Materials and Methods

2.1. Materials

Punica granatum, a plant that is indigenous to Periyakulam town in the Theni district of Tamilnadu state, India, was harvested for its fresh stems. Sigma-Aldrich Germany provided reagent grade Zn $(CH_3COO)_2$. $2H_2O$ with a purity of 98 percent. No further purification was performed; all reagents were used as received.

2.2. Preparation of aqueous stem extract

A single Punica granatum plant (fig.1) in the village of Periyakulam provided the fresh stems, which were repeatedly cleaned in deionized water to eliminate any debris. After being cleaned, the stems (fig.2) were dried in the sun for a few days before being blended into a fine powder and sieved to obtain stems of the same size. The fine powder was precisely weighed at 2g, transferred to a 250 mL beaker with 50ml of deionized water, and then heated for 30 minutes at a temperature of about 70 °C. The mixture was then filtered using Whatman No. 1 filter paper into a different beaker, and the extract that was created was chilled and stored in a cool location for use in the subsequent synthesis of ZnNPs.

Figure 1: Punica granatum plant

Figure 2: Punica granatum stems

2.3. Preparation of zinc nanoparticles

For the green method of making ZnNPs, a 1:10 mixture of zinc acetate dehydrate [Zn(CH3COO) 2.2H2O] and the aqueous stem extract of Punica granatum was used. After heating the mixture for 15 minutes at 70°C to produce a brown precipitate, it was then cooled to 60°C for 40 minutes. The mixture was centrifuged at 9000 rpm for 10 minutes after being left at room temperature for an entire night. To get rid of contaminants, the precipitate was thrice rinsed with deionized water. The resulting precipitates were ground up and subjected to characterization after being dried in an oven at 80°C for 9 hours.

3. Characterization techniques

Using a Jasco dual-beam spectrophotometer (model JASCO V-750, Japan), the samples UV-visible absorbance spectra were measured in the 200–800 nm range. The aqueous stem extract solution was combined with the zinc solution after the necessary dilution to create the ZnNPs solution. The absorbance of the nanoparticle solution compared to a control extract solution was measured, and an absorbance spectrum was obtained by enabling the instrument to scan wavelengths between 200 and 800 nm. The Tauc model has been used to compute the band gap. Using KBr pellets, Fourier transform infrared spectroscopy (FTIR) measurements were made in the 400–4000 cm-1 range using a JASCO FT/IR-4700 spectrophotometer. The produced nanomaterials' thermal properties were examined using thermo gravimetric and differential thermal analysis (TGA & DTA), which were calibrated for thermodynamic and kinetic parameters using the Coats and Redfern model.

The X-ray diffraction analysis (XRD) supports the morphological studies of produced nanomaterials. Scanning electron microscopy (SEM), transmission electron microscopy, and energy dispersive X-ray analysis (EDAX) were used to study the surface morphology and identify the components included in the produced nanomaterials. The

binding nature of each individual element present in the produced nanomaterials was validated by X-ray photoelectron spectroscopy (XPS). The Brunauer-Emmett-Teller (BET) test was used to assess the surface area, pore volume, and pore diameter.

4. Applications

4.1. Antimicrobial Evaluation

Utilising the Agar disc-diffusion method [15] and testing against gram positive (S. aureus, S pneumonia, Bacillus subtilis) and gram negative (Klebsiella pneumonia, E coli, pseudomonas aeruginosa) bacterial strains, the antibacterial activity of synthesised ZnNPs was assessed. Using the sterile swab, 100 mL of a fresh culture containing 1108 CFU/mL of bacteria was applied to the Mueller Hinton Agar (MHA) plates. A 40 l concentration of ZnNPs dispersed in DMSO was used to test the Petri-plate. Following this, zone of inhibition levels (mm) were monitored for 24 hours at 37°C. Standard antibiotic Streptomycin (10 g disc) was employed as a positive control. The test fungus C. albicans was used to investigate the antifungal activity on potato dextrose agar using a well diffusion method. First, potato dextrose broth (PDB) was added to the test strain, and it was cultured at 30°C. Then, using sterile forceps, a well filled with a 40 l test sample of ZnNPs was dropped onto the infected plate and incubated at 30 °C for 24 h while exposed to light.

4.2. Anticancer Activity

Cell viability assay, HeLa & SKMEL-3 viable cells were harvested and counted using haemocytometer diluted in DMEM medium to a density of 1 × 104 cells/ml was seeded in 96 well plates for each well and incubated for 24 h to allow attachment. After HeLa & SKMEL-3 cells treated with control and the containing different concentrations of (2.5 - 15 µg/mL) were applied to each well. HeLa & SKMEL-3 cells were incubated at 37°C in a humidified 95% air and 5% CO2 incubator for 24 h. After incubation, the drug-containing cells wash with fresh culture medium and the MTT (5 mg/mL in PBS) dye was added to each well, followed by incubated for another 4 h at 37°C. The purple precipitated formazan formed was dissolved in 100 µL of concentrated DMSO and the cell viability was absorbance and measured 540 nm using a multi-well plate reader. The results were expressed at the percentage of stable cells with respect to the control.

5. Results and Discussion

Aqueous Punica granatum stem extracts undergo physio-chemical alterations when zinc acetate solution is added. Within minutes, the reaction mixture's hue changes, which are the most noticeable alteration. This is seen as the first indication that NPs are forming. As ZnNPs formed, the coloration in the current study changed from yellow to dark brown. A few hours later, the solution's colour stopped shifting, indicating that Zn was completely bio reduced to ZnNPs. Fig.3 provides a vivid example of the reaction mixture's colour change as a result of Zn NP production. The outcomes are in line with other accounts of colour changes caused by plant-based ZnNP production [16]. Temperature is thought to be a key ingredient in the production of high-quality nanoparticles. The relationship between reaction temperature and nanoparticle size has been demonstrated [17, 18]. Therefore, the reactants were incubated at 60 °C, which caused the synthesis of small-sized ZnNPs.

Figure 3: Test tubes from left: Aqueous PG Stem extract, Zinc Acetate solution and Synthesized ZnNPs

5.1 UV-visible spectra of PG stem extract and ZnNPs

A popular technique for examining the optical characteristics of nanoparticles is UV- Vis spectroscopy. Figure 4 shows the UV-visible spectra of synthesised ZnNPs and PG stem extract. The absorption peak for the PG stem extract can be seen at 244, 276 and 361 nm, which indicates the occurrence of the π-π* and n-π* transitions. This demonstrates that the functional groups C=C and O-H are present in the plant extract. Similar to ZnNPs, PG stem extract and zinc metal interact in a way that has a maximal absorption band at 425 nm.

The energy difference between the valence and conduction bands (CB) is referred to as a material's band gap (BG). A substance will be more electrically conductive, smaller the band gap. The typical approach for estimating Eg from UV-Vis data (in the R, A, or T mode) is Tauc's plot. Through the Tauc model (an indirect method), the band gap of the PG stem extract and ZnNPs has been calculated (fig. 5). ZnNPs have a band gap of 4.70 eV, whereas PG stem extract has a band gap of 4.73 eV (figs. 6 and 7). The outcome makes it obvious that the band energy dropped as the UV radiation rose. A similar assumption was made by (Niu et al., 2003; Devendrappa et al., 2006) regarding the cause of this decrease in band gap, that caused more zinc ions to get reduced to ZnNPs.

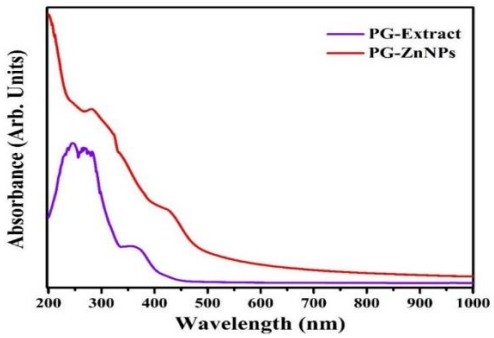

Figure 4: UV-Visible spectra of PG stem extract and ZnNPs

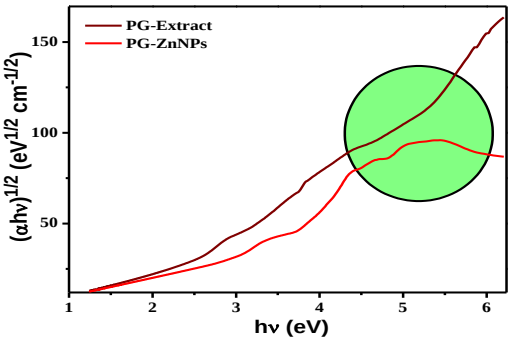

Figure. 5: Tauc's plot for the stem extract- ZnNPs

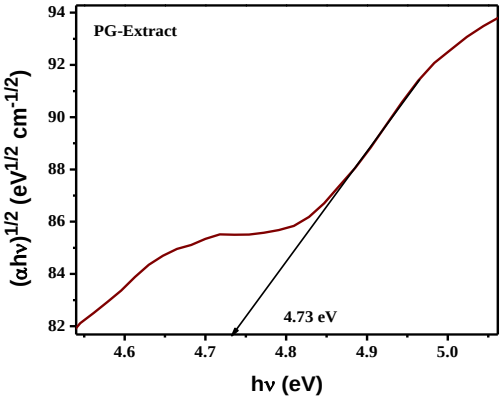

Figure 6: Tauc's plot for the PG stem extract

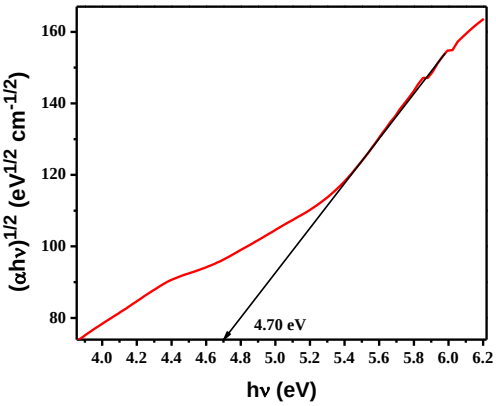

Figure 7: Tauc's plot for the ZnNPs

5.2 FTIR spectral studies

The numerous absorption bands are visible in the recorded FTIR spectra for PG stem extract and produced ZnNPs (fig.8). The -OH stretching frequency is shown by the band at 3339 cm^{-1}, while the C=O stretching frequency is indicated by the band at 1635 cm^{-1} in the PG stem extract. The ZnNPs' OH (alcoholic and phenolic) stretching frequency is described by the band at 3362 cm^{-1}. The presence of an amide functional group is represented by the band at 1568 cm^{-1}. The existence of CN stretching of aliphatic amide is suggested by the absorption band position at

1433 cm^{-1}. Stretching vibration's amino functional group and carboxylic acid are located at 1350, 1312, and 1017 cm^{-1}, respectively. The aromatic CH out of plane bending vibration is represented by the absorption band position at 825 cm^{-1}. The metal interaction between ZnNPs is represented by the strong absorption bands at 572 cm^{-1} [19, 20].

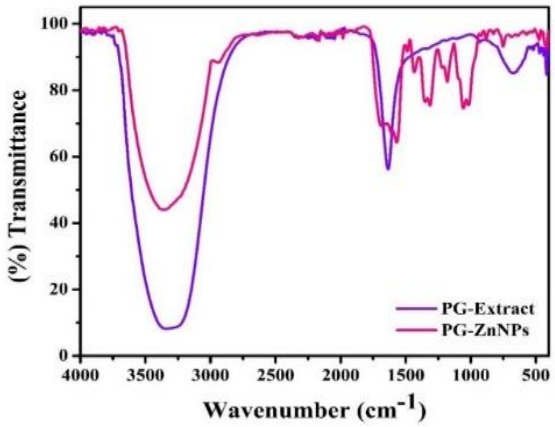

Figure 8: FT-IR spectra of PG stem Extract and ZnNPs

5.3 Scanning electronic microscopic studies and energy dispersive analysis of ZnNPs

5.3.1 Scanning electronic microscopic study of ZnNPs

The morphology and size of the newly synthesised ZnNPs were observed utilising the SEM method and an aqueous PG Stem extract. The ZnNP SEM images displayed (fig. 9) at 500 nm magnification showed an irregularly sized, rough surfaced spherical shape. The size of the nanoparticles determined using the image J tool indicated that the particle size ranged between 11 and 30 nm (fig.10).

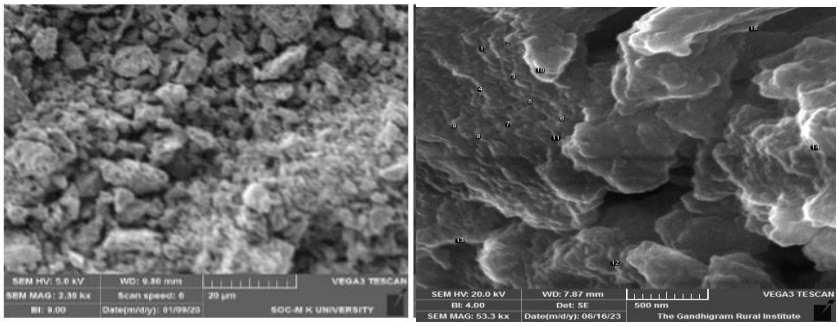

Figure 9: SEM images of PG-ZnNPs

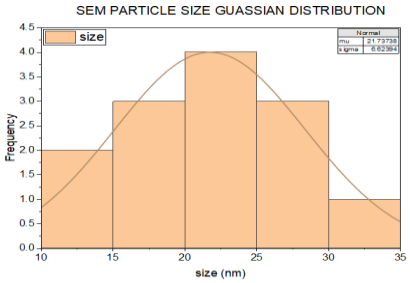

Figure 10: Histogram showing the particle size distribution in nm

5.3.2 Energy dispersive micro analysis of ZnNPs

The energy dispersive micro analysis method was used to investigate the elemental analysis of zinc nanoparticles. Peaks were found in the nanoparticle EDAX spectra (fig. 11) at energies of 0.25, 0.40, 0.50, 1 and 8.6 eV. The freshly synthesised ZnNPs contain zinc, carbon, nitrogen, and oxygen, as shown by the spectra.

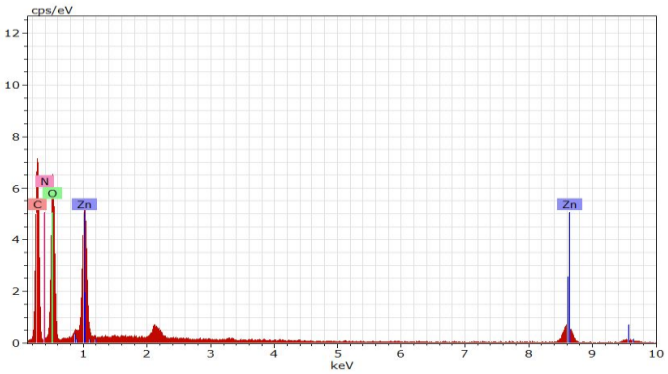

Figure 11 EDAX spectrum of PG-ZnNPs

5.4 Transmission Electron Microscopy (TEM)

The TEM pictures (fig. 12) of the synthesised Zn NPs also demonstrate the formation of spherical and flower-shaped nanoparticles, with diameters ranging from 5 to 22 nm. The presence of polyphenolic chemicals from the aqueous stem extract of Punica Granatum, which serve as a capping agent, may explain the weak thin coating that surrounds the surface of zinc nanoparticles.

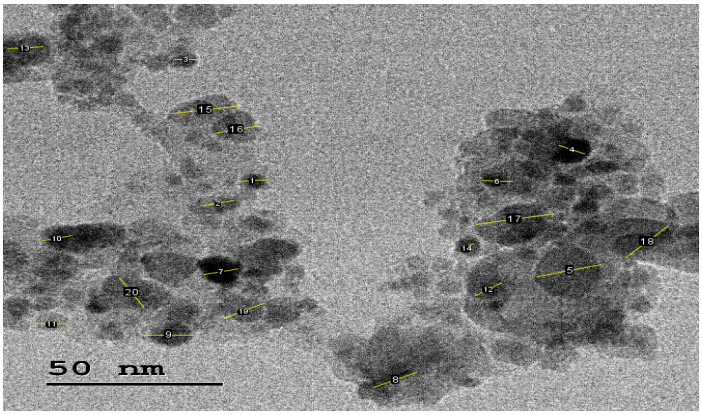

Figure 12: TEM Images of Synthesized ZnNPs

5.5 XRD Analysis

The nature of ZnNPs was verified using X-ray diffraction investigation. For the XRD analysis, powdered dry ZnNPs were employed. The XRD pattern (fig.13) of the synthesised ZnNPs showed the 2θ values at 12.13, 16.78, 17.01, 19.05, 19.95, 21.08, 22.06, 25.16, 26.74, 28.26, 32.19, 33.09, 35.58, 39.89, 43.29, 46.01, 51.8, 60.74, 67.76 and 70.03° and the comparison of the XRD spectrum with the standard confirmed that ZnNPs formed were in the nano crystal form. The JCPDS No. 33-1464 was perfectly matched by all of the relevant 2 values. The face-centered cubic (FCC) crystalline structure of the ZnNPs synthesised using aqueous stem extract of Punica granatum as the reducing and stabilising agent was revealed by X-ray diffraction analysis depicted in fig. 13; 28.26, 39.89, 43.29, 67.76, and 70.03 at 2h angle, which matched to 110, 111, 200, 220, and 311. A high amount of crystallinity is indicated by the prominent peak at 39.89 [21, 22]. According to Krishnaraj et al.'s research [23], the presence of phytochemical substances in the plant's aqueous extract may have coated the surface of the synthesised ZnNPs and stabilised them, as evidenced by the high peaks at 32.19 and 43.29 in the XRD spectra. Other unidentified peaks seen in the XRD spectra may be due to the presence of some organic compounds derived from the Punica granatum aqueous stem extract [24]. Our results are consistent with those of Carmona et al. [25] and Kamaraj et al. [26], who found that the XRD peaks of the biosynthesized ZnNPs matched those of cubic crystalline zinc at (111), (200), (220), and (311).

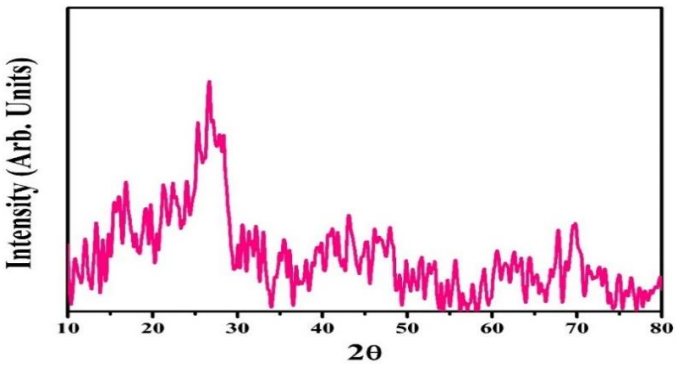

Figure 13: XRD pattern of PG-ZnNPs

5.6 Thermogravimetric Analysis of ZnNPs

The weight loss values and the freshly synthesised ZnNPs thermogram at various heating rates are summarised in Table 1 (fig. 14 [A-F]). The thermogravimetric analysis shows the three-stage deterioration. The manufactured ZnNPs lost moisture at different heating rates of 10, 20, 30, 40, and 50 °C and in that order, which resulted in weight losses of 13.75, 12.16, 10.60, 8.50, and 6.72% during the first stage of decomposition at temperatures between 30 and 100 °C. Due to the loss of alkaloid, flavonoids, triterpene acid, and hemicellulose present in the ZnNPs, the second stage weight loss was expected to range from 100 to 450 °C, and the weight loss was reported to be 31.34, 38.16, 33.10, 35.83, and 33.25% at heating rates of 10, 20, 30, 40, and 50 °C, respectively [27]. Due to the loss of ZnNPs, the third stage weight loss of 19.75, 21.27, 23.29, 21.35, and 20.10% was seen at heating rates of 10, 20, 30, and 50 °C, respectively, and was seen at temperatures between 450-800 °C.

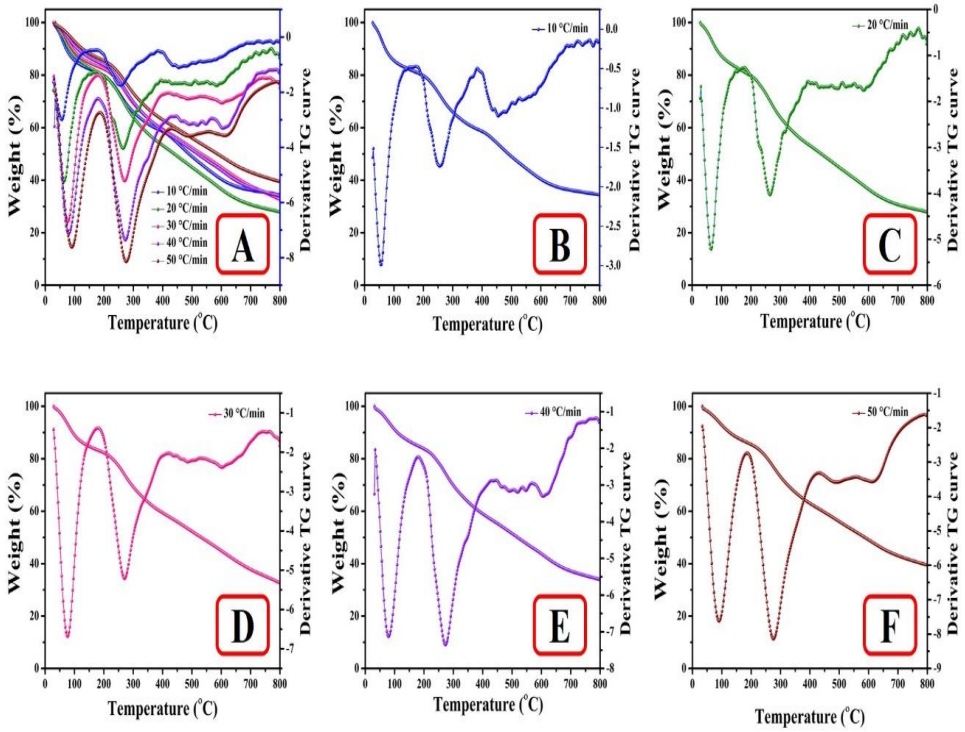

Figure 14: Thermogram of ZnNPs of different heat rate A) Overall heating rate (10 – 50 °C) B) ZnNPs 10 °C/min, C) ZnNPs 20 °C/min, D) ZnNPs 30 °C/min, E) ZnNPs 40 °C/min, F) ZnNPs 50 °C/min

Table 1: The weight loss of PG-ZnNPs at different heating rate (10 – 50 °C)

S. No.	Heating Rate (°C/min)	Temperature (°C) Weight loss (%)			Total weight loss (%)	Residue (%)
		30 - 100	100 - 450	450 - 800	30 - 800 (°C)	
1	10	13.75	31.34	19.75	64.84	35.16
2	20	12.16	38.16	21.27	71.59	28.41
3	30	10.60	33.10	23.29	66.99	33.01
4	40	8.50	35.83	21.35	65.68	34.32
5	50	6.72	33.25	20.10	60.07	39.93

The disintegration of the ZnNPs causes the weight loss to vary depending on the heating rate, and the total weight loss was seen between 30 and 800 °C. At various heating rates of 10, 20, 30, 40, and 50 °C, weight losses of 64.84, 71.59, 66.99, 65.68, and 60.07%, respectively, occurred. At a heating rate of 50 °C/min, the highest residue was detected at a rate of 39.93%. Figure 15 [A - F] shows the curve of ln [-ln (1 - x)] vs. 1000/T at different heating rates for PG-ZnNPs. Through thermal analysis at varied heating rates of 100 ° C (Phase I), 250 °C (Phase II), and 600 °C (Phase III), newly synthesised ZnNPs' activation energy (Ea.), free energy (G), enthalpy (H), and entropy (S) were calibrated. The resulting values are listed in Table 2. The diverse heating rates of ZnNPs produced revealed positive values for the Gibbs free energy in the range of 94.7928 to 240.2731 kJ mol-1, indicating that the process is thermally non-spontaneous. The lowest value of G was 94.7928 kJ mol-1 in Phase I, measured at a heating rate of 10 °C/min.

The negative values of change in entropy (S) observed in Phase I and Phase II range from -0.1270 to -0.2811 kJ mol-1, respectively, and are heated at a rate of 10 °C/min. Enthalpy (H) positive values are seen between 1.7600 and 47.4382 kJ mol-1. The heating rate of 10 °C/min from Phase I results in the lowest and highest values of H. At a heating rate of 10°C/min from Phase I, the highest and lowest Ea values of 50.5394 and 6.1083 kJ mol-1 are recorded.

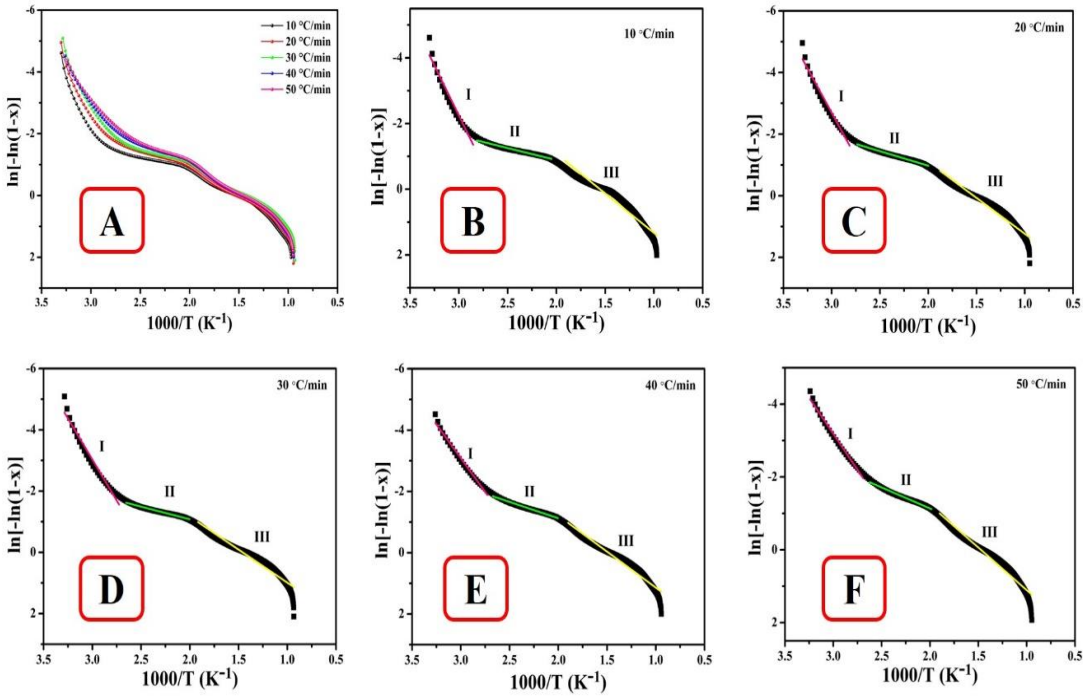

Figure 15: Plot of ln [-ln (1 - x)] vs 1000/T at different heating rate PG-ZnNPs A) Overall heating rate (10 – 50 °C), B) PG-ZnNPs 10 °C/min, C) PG-ZnNPs 20 °C/min, D) PG-ZnNPs 30 °C/min, E) PG-ZnNPs 40 °C/min, F) PG-ZnNPs 50 °C/min

Table 2 Thermodynamic parameters of PG-ZnNPs at different heating rate at temperature (100, 250 and 600 ° C)

S. No	Heating rate (°C/min)	phase	Temp. (°C)	Ea (kJ mol^{-1})	ΔS (kJ mol^{-1})	ΔH (kJ mol^{-1})	ΔG (kJ mol^{-1})
		I	100	50.5394	-0.1270	47.4382	94.7928
1	10	II	250	6.1083	-0.2811	1.7600	148.7554
		III	600	19.9751	-0.2578	12.7167	237.7916
		I	100	47.7721	-0.1392	44.6708	96.5768
2	20	II	250	7.8373	-0.2760	3.4889	147.8222
		III	600	19.3618	-0.2592	12.1034	238.3718
		I	100	44.5346	-0.1520	41.4334	98.1164
3	30	II	250	6.8826	-0.2795	2.5342	148.7345
		III	600	17.9352	-0.2630	10.6768	240.2731
		I	100	36.6685	-0.1774	33.5672	99.7277
4	40	II	250	8.8864	-0.2735	4.5380	147.5942
		III	600	19.5116	-0.2592	12.2532	238.5482
		I	100	32.8614	-0.1903	29.7601	100.7387
5	50	II	250	9.6080	-0.2713	5.2596	147.1335
		III	600	19.4255	-0.2594	12.1671	238.5870

5.7 Differential Thermal Analysis

One of the most popular techniques for identifying chemicals and researching a material's thermal stability is thermal analysis [29, 30]. The endothermic values listed in Table 3 are displayed in Fig. 16 of the differential thermal analysis of ZnNPs. The ZnNPs exhibit two endothermic peaks with peak temperatures between 60.30 and 102 °C (Peak 1), 218.40 and 238.80 °C (Peak 2). The endothermic curve at these ranges is between 1.87 and 10.13 J/g at Peak 2 and between 28.31 and 89.46 J/g at Peak 1. Peak 1 maximum heat was 89.46 J/g at 30 °C/min heating rate, and peak 2 was 10.13 J/g at 20 °C/min heating rate.

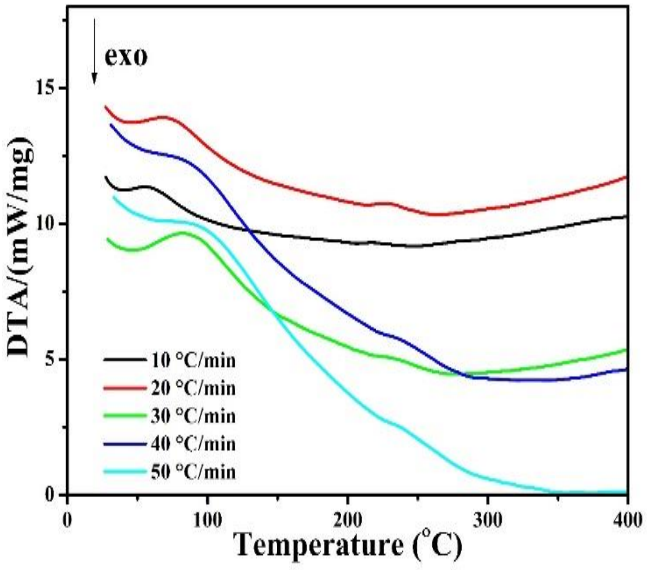

Figure 16: Differential Thermogram of PG-ZnNPs

Table 3: The Endothermic peaks area of PG-ZnNPs

S. No.	Heating rate (°C/min)	Peak1		Peak 2	
		Temp. (°C)	Area (J/g)	Temp. (°C)	Area (J/g)
1	10	60.30	54.13	218.40	5.28
2	20	60.71	60.71	229.40	10.13
3	30	86.90	89.46	232.30	3.18
4	40	89.90	28.31	235.70	2.86
5	50	102.00	31.26	238.80	1.87

5.8 BET ANALYSIS

ZnNPs were subjected to a BET analysis in order to learn more details about the nanoparticles' surfaces that were discovered using a Brunauer-Emmett-Teller (BET) analysis of a particular surface area. The BET analysis of ZnNPs revealed that at room temperature, the biogenic ZnNPs had a surface area of 4.10 m^2/g, a pore volume of 0.004 cc/g, and a pore diameter of 2.56 nm. The very small pore diameter and surface area may have an impact on the antibacterial activity.

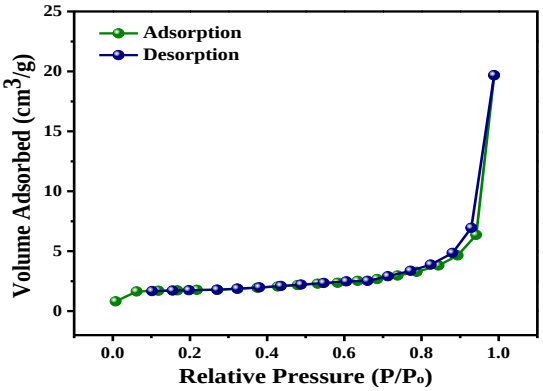

Figure 17: N_2 adsorption and desorption isotherm of PG-ZnNPs

5.9 XPS SURVEY SPECTRA

To investigate the oxidation status of ZnNPs, XPS measurements were made (fig. 18). The survey spectrum of ZnNPs was produced using stem extract from *Punica granatum* in a volume of 5% and zinc acetate dihydrate at a concentration of 1 mM. demonstrate that the spectrum solely contains the elements C, N, O, and Zn. The primary peaks, which are found at 286.08, 402.04, 533.08, and 1023.08, respectively, show the presence of C 1s (70.09%), N 1s (0.62%), O 1s (28.06%), and Zn 2p (1.13%).

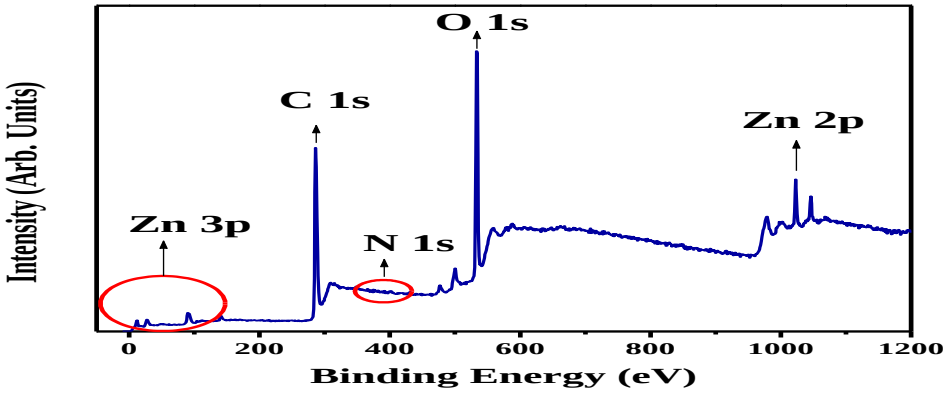

Figure 18: XPS Survey spectra of PG-ZnNPs

The newly synthesised C=O/C-O, C-N/C=N, and C=O functional groups can be seen in the C 1s core level spectra (fig. 19), which are situated at 286.60 (34.74%), 285.03 (46.52%), and 288.51 (18.75%) eV, respectively.

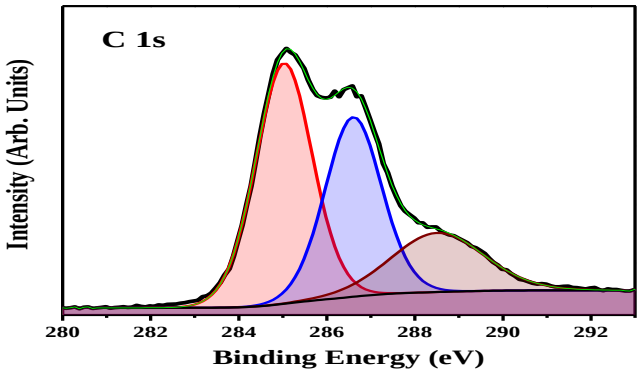

Figure 19: C 1s Core level spectra of PG-ZnNPs

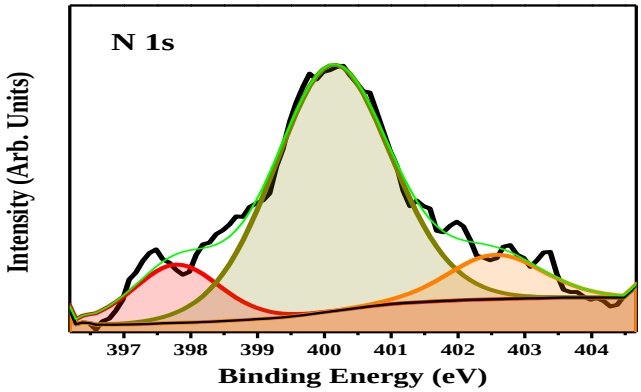

Figure 20: N 1s Core level spectra of PG-ZnNPs

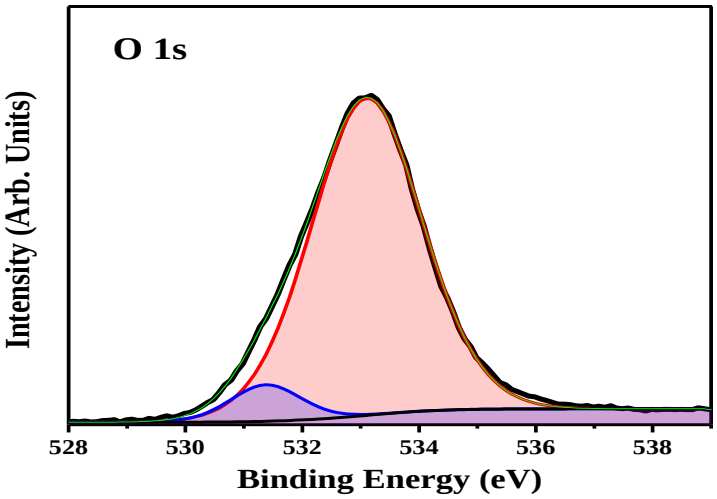

Figure 21: O 1s Core level spectra of PG-ZnNPs

Figures 20 and 21 display the N 1s and O 1s Core level spectra, respectively. The three components of the N 1s core level spectra are at 397.78 (13.24%), 400.12 (75.73%), and 402.56 (11.03%) eV. The ZnNPs contain the binding energies for N-H (397.78 eV) and N+ (400.78 and 402.55 eV) [30, 31].

The C-OH and C-O-C groups are present in the PG-ZnNPs, as shown by the O 1s core level spectra recorded of two component and position at 531.38 eV (6.78%) and 533.10 eV (93.22%) [32, 33].

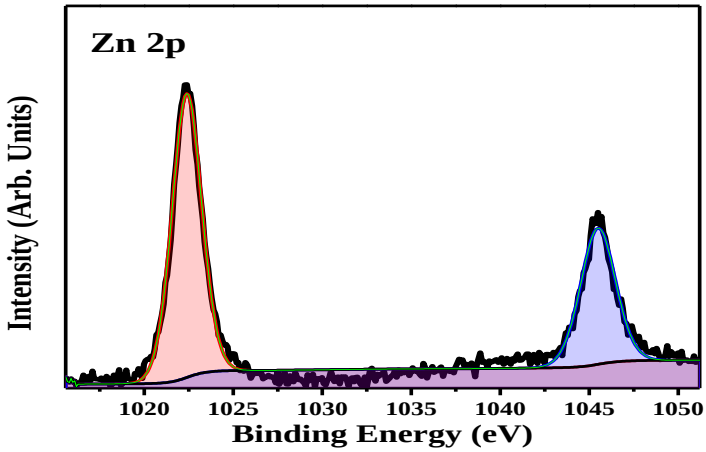

Figure 22: Zn 2p Core level spectra of PG-ZnNPs

The Zn 2p core level spectra are displayed (fig.22) and show the two components at 1022.38 and 1045.49 eV, respectively. This clearly illustrates the presence of Zn 2p3/2 and Zn 2p1/2 in ZnNPs [34].

5.10 Antimicrobial Activity

With concentrations ranging from 10 to 40 g/mL, the newly synthesised ZnNPs antibacterial activity is demonstrated (fig. 23) and estimated against various bacterial strains and a fungal strain. The results are listed in Table 4. Undoubtedly, the zinc cations released by ZnNPs cause the alterations in germ membrane structures, which in turn cause the bacteria's membrane permeability to increase and ultimately result in cell death.

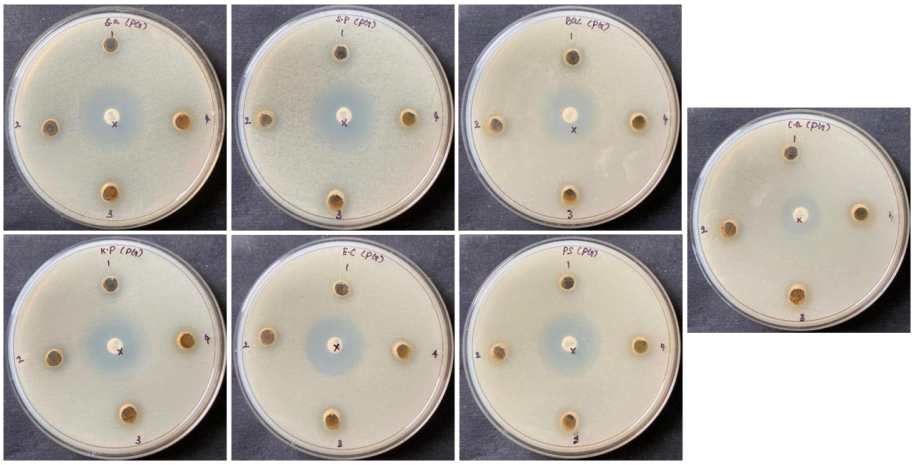

Figure 23 Antimicrobial activity of PG-ZnNPs

Table 4: Antimicrobial activity data of PG-ZnNPs at various bacteria and different concentration

S. No.	Bacteria Name	1 10 µg/mL	2 20 µg/mL	3 30 µg/mL	4 40 µg/mL	Streptomycin
1	*S. aureus*	11	12	12.5	13	24
2	*S. pneumoniae*	11	12	13	13.5	25
3	*B. subtilis*	8	8.5	9	10	20
4	*K. pneumoniae*	10	11	11.5	12	26
5	*E. coli*	8.5	9	10.5	11.5	23
6	*P. aeruginosa*	8	8.5	9	10	21
7	*C. albicans*	8	8.5	9.5	11	(Fluconazole) 16

At different concentrations of 10, 20, 30, and 40 g/mL, the inhibitory zone diameter (fig. 24) found against S. aureus was 11 mm, 12 mm, 12.5 mm, and 13 mm. ZnNPs demonstrated the greatest inhibition zone when tested against S. pneumoniae, with a diameter of 13.5 mm at the maximum concentration (40 g/mL) and 11 mm at the lowest tested dose (10 g/mL). The inhibitory zone diameters for B. subtilis were similar, measuring about 8 mm, 8.5 mm, 9 mm.

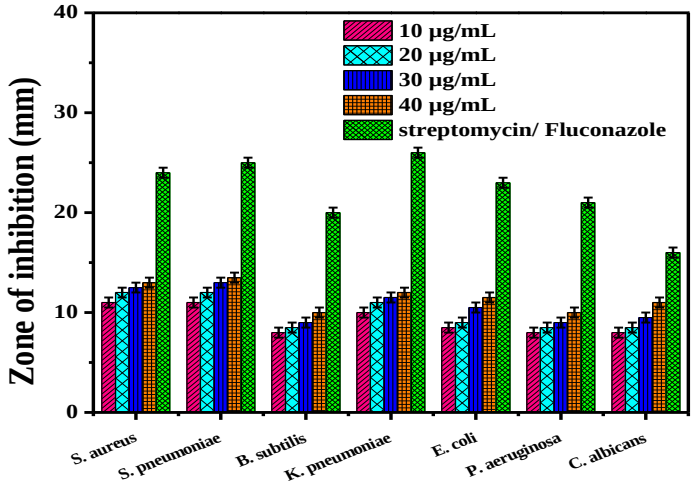

Figure 24: Antimicrobial activity with Zone inhibition of PG-ZnNPs

Additionally, when tested against gram-negative bacteria, ZnNPs showed antibacterial action against K. pneumoniae with inhibitory zone diameters between 10 and 12 mm at the appropriate dosages. ZnNPs displayed 8.5 mm to 11.5 mm against E. coli at various doses (10–40 g/mL). At various tested doses, another gram-negative P. aeruginosa bacteria caused an inhibitory zone diameter of 8 mm to 10 mm. Candida albicans, a fungus with an inhibitory zone diameter of around 8 mm to 11 mm at concentrations of 10–40 g/mL, showed a similar trend of inhibition. The inhibitory zone diameter of the common antibiotic streptomycin ranged from 20 to 26 mm, while that of fluconazole was 16 mm.

5.11 Anti-Cancer Activity

Studies have been done on the anticancer activity of ZnNPs (fig.25) against cervical cancer, skin cancer, SKMEL-3 and HeLa cell lines. When we increased the ZnNPs content from 2.5 to 15 g/mL, both HeLa and SKMEL-3 cell viability dropped. The results for the cell viability observed in HeLa against cervical cancer are 85.40 (4.09), 71.67 (2.68), 50.35% (2.85), 38.05 (5.66), 22.74 (4.64), and 14.87% (1.73), respectively, for 2.5, 5, 7.5, 10, 12.5 and 15 g/mL. 7.5, 10, 12.5 and 15 g/mL.

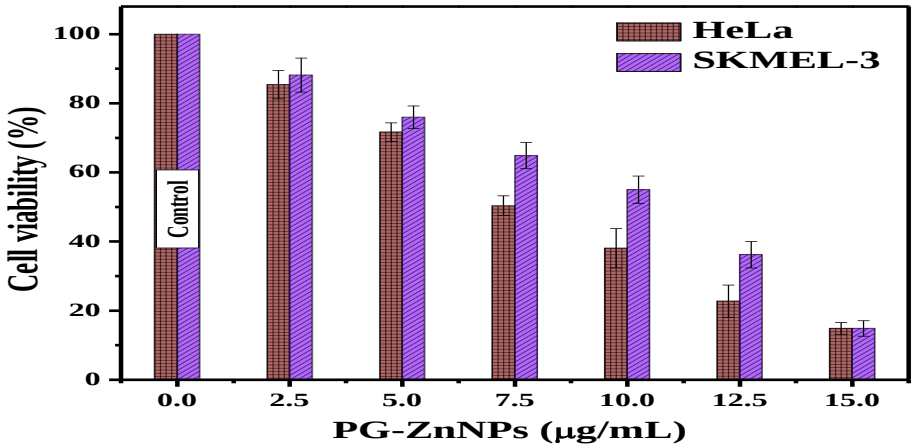

Figure 25: Anticancer activity of PG-ZnNPs against HeLa and SKMEL-3 cell

Similar results were obtained for SKMEL-3's cell viability against skin cancer, with values of 88.17 (4.92), 75.98 (3.24), 64.87% (3.81), 55.01 (3.96), 36.20 (3.81), and 14.87% (2.23) for concentrations of 2.5, 5, 7.5, 10, and 12.5 g/mL, respectively. The morphological alterations in HeLa and SKMEL-3 cell cervical and skin cancer reflect the control of HeLa cell cervical cancer for ZnNPs concentrations of 10 and 12.5 g/mL at 24 hours, respectively (fig.26 [A-C] and fig.27 [A-C]). In the fig. 27, A, B and C signifies the control of skin cancer of SKMEL-3 for At 24 hours, the concentration of ZnNPs was 7.5 and 10 g/mL, respectively. The findings support ZnNPs' strong anticancer effect against cervical cancer and skin cancer in HeLa and SKMEL-3 cells. Both cancer cells accelerate similarly at the greater concentration (15 g/mL), as seen by the almost identical value.

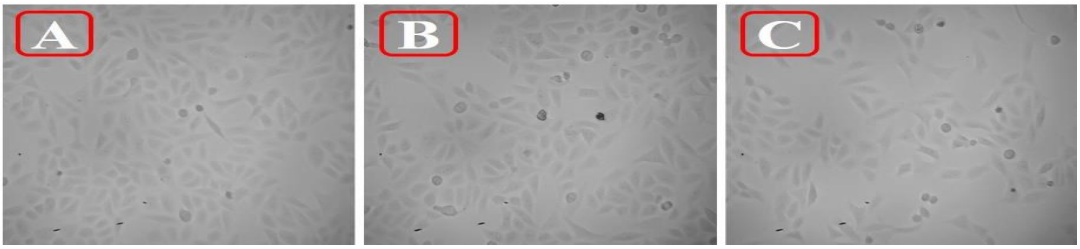

Figure 26: Morphological changes in cervical cancer of HeLa cell against PG-ZnNPs
A) Control B) 10 µg/mL C) 12.5 µg/mL at 24 Hrs

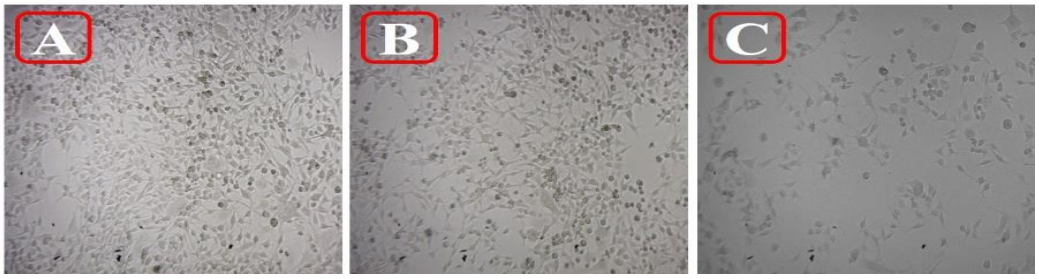

Figure 27: Morphological changes in skin cancer of SKMEL-3 cell against PG-ZnNPs
A) Control B) 7.5 µg/mL C) 10 µg/mL at 24 Hrs

6. Conclusions

The creation of non-toxic, biocompatible, and environmentally friendly nanoparticle production techniques is urgently required. It has been demonstrated that compared to other creatures, plants create metal nanoparticles that are more stable. More quickly than fungus or bacteria, plants (and especially plant extracts) are able to decrease metal ions. Plant extracts are more effective for the commercial manufacture of well-dispersed metal nanoparticles than plant biomass or microbes. Researchers have concentrated their efforts on discovering and characterising the biomolecules involved in the creation of metallic nanoparticles as well as studying the biological mechanisms and enzymatic processes of nanoparticle formation. Proteins/enzymes, amino acids, polysaccharides, alkaloids, alcoholic compounds, and vitamins are just a few examples of the many biomolecules found in plants that may be involved in the bio reduction, synthesis, and stabilisation of metal nanoparticles.

The use of biologically produced zinc metal nanoparticles has proven to be quicker, cleaner, and more environmentally friendly than physical and chemical approaches. The Punica granatum aqueous stem extract was used to create new, widely used zinc nanoparticles. The freshly synthesised zinc nanoparticles have been characterised using methods like UV-visible spectroscopy, SEM, TEM, XRD, DTA/TGA, BET, and XPS. SEM and TEM analyses verified that the synthesised ZnNPs had a size range of 11 to 30 nm. The aqueous stem extract of PG was used to create Zn nanoparticles, which have effective anti-cancer properties as well as potential antibacterial activity against microorganisms.

References

[1]. Hofmann MR, Martin ST, Choi W, Bahnemann (1995) DW. Environmental applications of semiconductor photocatalysis. Chem Rev.; 95: 69–96. https://doi.org/10.1021/cr00033a004.

[2]. Huang X, El-Sayed IH, Qian W, El-Sayed MA. (2006) Cancer cell imaging and photothermal therapy in the near-infrared region by using gold nanorods. J Am Chem Soc.; 128:2115–20. https://doi.org/10.1021/ja057254a.

[3]. Kim JS, Kuk E, Yu KN, et al. (2006) Antimicrobial effects of silver nanoparticles. Nanomed Nanotechnol Biol Med. 2007; 3:95–101. https://doi. org/10.1016/j.nano.12.001.

[4]. Laurent S, Forge D, Port M, et al. (2008) Magnetic iron oxide nanoparticles: synthesis, stabilization, vectorization, physicochemical characterizations, and biological applications. Chem Rev.; 108: 2064–110. https ://doi.org/10.1021/cr068445e.

[5]. Livage J, Henry M, Sanchez C. (1988) Sol–gel chemistry of transition metal oxides. Prog Solid-State Chem.; 18:259–341. https://doi. org/10.1016/0079-6786(88)90005-2.

[6]. O'Neal DP, Hirsch LR, Halas NJ, et al. (2004) Photo-thermal tumor ablation in mice using near infrared-absorbing nanoparticles. Cancer Lett. 2016; 209:171–6. https://doi.org/10.1016/j.canlet.02.004.

[7]. Oskam G. Metal oxide nanoparticles: synthesis, characterization and application. J Sol–gel Sci Technol. 2006; 37:161–4.

[8]. Sastry M, Ahmad A, Khan MI, Kumar R.(2003) Biosynthesis of metal nanoparticles using fungi and actinomycete. Curr Sci.; 85:162–70. https:// doi.org/10.1016/S0927-7765(02) 00174-1.

[9]. Su X-Y, Liu P-D, Wu H, Gu N. (2014) Enhancement of radiosensitization by metal-based nanoparticles in cancer radiation therapy. Cancer Biol Med.;11:86–91. https://doi.org/10.7497/j.issn.2095-3941.2014.02.003.

[10]. Dagdeviren, C., Hwang, S.W., Su, Y., Kim, S., Cheng, H., Gur, O., Haney, R., Omenetto, F. G., Huang, Y. and Rogers, J.A. (2013) Transient, Biocompatible Electronics and Energy Harvesters Based on ZnO. Small , 9, 3398-3404. http://dx.doi.org/10.1002/smll.201300146

[11]. Wang, L., Kang, Y., Liu, X., Zhang, S., Huang, W. and Wang, S. (2012) ZnO Nanorod Gas Sensor for Ethanol Detection. Sensors & Actuators, B: Chemical, 162, 237-243. http://dx.doi.org/10.1016/j.snb.2011.12.073

[12]. Cross, S.E., Innes, B., Roberts, M.S., Tsuzuki, T., Robertson, T.A. and McCormick, P. (2007) Human Skin Penetration of Sunscreen Nanoparticles: In - Vitro Assessment of a Novel Micronized Zinc Oxide Formulation. S kin Pharmacology and Physiology, 20, 148-154. http://dx.doi.org/10.1159/000098701

[13]. Zhou, J., Xu, N. and Wang, Z.L. (2006) Dissolving Behavior and Stability of ZnO Wires in Biofluids: A Study on Biodegradability and Biocompatibility of ZnO Nanostructures. A dvanced Materials, 18, 2432-2435. http://dx.doi.org/10.1002/adma.200600200

[14]. Rasmussen, J.W., Martinez, E., Louka, P. and Wingett, D.G. (2010) Zinc Oxide Nanoparticles for Selective Destruction of Tumor Cells and Potential for Drug Delivery Applications. Expert Opinion on Drug Delivery, 7, 1063-1077. http://dx.doi.org/10.1517/17425247.2010.502560

[15]. S. Manandhar, S. Luitel, and R. K. Dahal, (2019) "In vitro antimicrobial activity of some medicinal plants against human pathogenic bacteria," Journal of Tropical Medicine, Article ID 1895340, 5 pages, 2019.

[16]. Rajiv, P., Rajeshwari, S. & Venckatesh, R. (2013), Bio-Fabrication of zinc oxide nanoparticles using leaf extract of Parthenium hysterophorus L. and its size-dependent antifungal activity against plant fungal pathogens. Spectrochimica Acta Part A: Mol. Biomol. Spectr. 112, 384–387.

[17]. Saware, K. & Venkataraman, A. (2014), Biosynthesis and characterization of stable silver nanoparticles using Ficus religiosa leaf extract: A mechanism perspective. J. Clust. Sci. 25, 1157–1171.

[18]. Jain, S. & Mehata, M. S. (2017), Medicinal plant leaf extract and pure flavonoid mediated green synthesis of silver nanoparticles and their enhanced antibacterial property. Sci. Rep. 7, 15867, https://doi.org/10.1038/s41598-017-15724-8.

[19]. A.Y. Ghidan, T.M. Al-Antary, A.M. Awwad (2016), Green synthesis of copper oxide nanoparticles using Punica granatum peels extract: Effect on green peach Aphid, Environ. Nanotechnology, Monit. Manag. 6, 95–98. doi:10.1016/j.enmm.2016.08.002.

[20]. P. Kaur, R. Thakur, A. Chaudhury, (2016), Biogenesis of copper nanoparticles using peel extract of Punica granatum and their antimicrobial activity against opportunistic pathogens, Green Chem. Lett. Rev. 9, 33–38. doi:10.1080/17518253.2016.1141238.

[21]. S. Pattanayak, M. M. R. Mollick, D. Maity, S. Chakraborty, S. K. Dash, S. Chattopadhyay, S. Roy, D. Chattopadhyay, and M. Chakraborty, (2017) J. Saudi Chem. Soc. 21, 673.

[22]. N. Basavegowda and Y. Rok-Lee, (2014), Mater. Lett. 109, 31.

[23]. C. Krishnaraj, E. G. Jagan, S. Rajasekar, P. Selvakumar, P. T. Kalaichelvan, and N. Mohan, (2010), Colloid Surf. B Biointerfaces 76, 50.

[24]. D. Kumar, G. Kumar, R. Das, and V. Agrawal, (2018), Process Saf. Environ. 116, 137.

[25]. E. R. Carmona, N. Benito, T. Plaza, and G. Recio-Sa´nchez, (2017), Green Chem. Lett. Rev. 10, 250.

[26]. C. Kamaraj, G. Balasubramani, C. Siva, M. Raja, V. Balasubramanian, R. K. Raja, S. Tamilselvan, G. Benelli, and P. Perumal, (2017), J. Clust. Sci. 28, 1667.

[27]. M.M. Sharrif, H.K. Hamed, (2012), Chemical composition of the plant Punica granatum L. (Pomegranate) and its effect on heart and cancer, J. Med. Plants Res. 6, 5306–5310. doi:10.5897/jmpr11.577.

[28]. S. Golczak, A. Kanciurzewska, M. Fahlman, K. Langer, J.J. Langer, (2008), Comparative XPS surface study of polyaniline thin films, Solid State Ionics. 179, 2234–2239. doi:10.1016/j.ssi.2008.08.004.

[29]. R. Atchudan, T.N.J.I. Edison, S. Perumal, N. Clament Sagaya Selvam, Y.R. Lee, (2018), Green synthesized multiple fluorescent nitrogen-doped carbon quantum dots as an efficient label-free optical nanoprobe for in vivo live-cell imaging, J. Photochem. Photobiol. A Chem. 372, 2019, 99–107. doi:10.1016/j.jphotochem.12.011.

[30]. R. Ullah, G.A. Bowmaker, C. Laslau, G.I.N. Waterhouse, Z.D. Zujovic, K. Ali, A.U.H.A. Shah, J. Travas-Sejdic, (2014), Synthesis of polyaniline by using CuCl2 as oxidizing agent, Synth. Met. 198, 203–211. doi:10.1016/j.synthmet.2014.10.005.

[31]. S. Palaniappan, S. Ajit, (2011), Preparation of processible polyaniline-formate salt via emulsifier free inverted emulsion polymerization and its antistatic applications, Synth. Met. 161, 1029–1033. doi:10.1016/j.synthmet.2011.03.011.

[32]. T.N.J.I. Edison, R. Atchudan, M.G. Sethuraman, J.J. Shim, Y.R. Lee, (2016) Microwave assisted green synthesis of fluorescent N-doped carbon dots: Cytotoxicity and bio-imaging applications, J. Photochem. Photobiol. B Biol. 161, 2016, 154–161. doi:10.1016/j.jphotobiol...05.017.

[33]. M.R. Pacquiao, M.D.G. de Luna, N. Thongsai, S. Kladsomboon, P. Paoprasert, (2018) Highly fluorescent carbon dots from enokitake mushroom as multi-faceted optical nanomaterials for Cr6+ and VOC detection and imaging applications, doi:10.1016/j.apsusc.2018.04.199.

[34]. A. Khataee, S. Saadi, M. Safarpour, S.W. Joo, (2015), Sonocatalytic performance of Er-doped ZnO for degradation of a textile dye, Ultrason. Sonochem. 27 379–388. doi:10.1016/j.ultsonch.2015.06.010.

[35]. Ismail K, Zakaria Z, Ishak MAM. (2005), Thermal behaviour study of Mukah Balingian coal and biomass blend during pyrolysis via thermogravimetric analysis. In: Paper Presented at the 22nd International Pittsburgh Coal Conference, Pittsburgh USA.

[36]. Vuthaluru H. (2004), RETRACTED: Investigations into the pyrolytic behaviour of coal/biomass blends using thermogravimetric analysis. In: Elsevier.